INTERNATIONAL JOURNAL FOR NUMERICAL METHODS IN FLUIDS
Int. J. Numer. Meth. Fluids 2009; **59**:1111–1124
Published online 17 June 2008 in Wiley InterScience (www.interscience.wiley.com). DOI: 10.1002/fld.1860

Optimal control of film casting processes

K. Selvanayagam[1,*,†], Thomas Götz[2], S. Sundar[1] and V. Vetrivel[1]

[1]*IIT Madras, Chennai 600036, India*
[2]*TU Kaiserslautern, Germany*

SUMMARY

We present an optimal control approach for the isothermal film casting process with free surfaces described by averaged Navier–Stokes equations. We control the thickness of the film at the take-up point using the shape of the nozzle and the initial thickness. The control goal consists in finding an even thickness profile. To achieve this goal, we minimize an appropriate cost functional. The resulting minimization problem is solved numerically by a steepest descent method. The gradient of the cost functional is approximated using the adjoint variables of the problem with fixed film width. Numerical simulations show the applicability of the proposed method. Copyright © 2008 John Wiley & Sons, Ltd.

Received 12 February 2008; Revised 7 May 2008; Accepted 9 May 2008

KEY WORDS: film casting process; optimal control; first-order optimality system; adjoint system; numerical simulation; edge-bead defect

1. INTRODUCTION

Polymer films for video and magnetic tapes are produced by film casting. The molten polymer emerging from a flat die is first stretched a short distance between the die and a temperature-controlled roll. The film shows a lateral neck-in as well as an inhomogeneous decrease in the thickness. The formation of edge beads surrounding a central area of constant thickness is generally called the dog bone defect or edge-bead defect. In this paper we develop a mathematical model to predict the shape of the die, which minimizes the edge-bead defect.

This paper is organized as follows: In Section 2 we explain the mathematical model describing the film casting process in an isothermal situation. In Section 3, the first-order optimality system is introduced. Numerical methods and simulation results for both the state system and the optimization problem are presented in Section 4. We conclude with an outlook on open questions for future research.

*Correspondence to: K. Selvanayagam, IIT Madras, Chennai 600036, India.
†E-mail: kselva@iitm.ac.in

2. MODELLING FILM CASTING PROCESSES

In this paper we consider the stationary three-dimensional Newtonian, isothermal model for the film casting process, derived earlier by Demay and co-workers [1–3] and Barq *et al.* [4]. The geometry of the film casting process is shown in Figure 1. During the film casting process, polymer is pressed through a nozzle or a die (located in the yz-plane) with a velocity u_0 and wrapped up (velocity $u_L > u_0$) by a spindle at $x = L$. The nozzle has a width of W_0 in the y-direction and a thickness of e_0 in the z-direction. For typical film casting processes, the thickness of the film at the nozzle is small compared with both the length and the width of the film, i.e. $e_0/W \ll 1$ and $e_0/L \ll 1$. In this thin film limit, the velocity component in the z-direction is small and hence we neglect it. The velocity components u and v in the xy-plane weakly vary with the z-coordinate and hence we assume a two-dimensional flow. Averaging the mass and momentum equations over the z-direction leads to the following reduced equations:

$$\nabla \cdot (eU) = 0 \tag{1a}$$

$$(U \cdot \nabla)U = \frac{1}{Re}(\Delta U + 3\nabla(\nabla \cdot U)) \tag{1b}$$

where $U = (u, v)$ denotes the velocity field in the x- and y-directions and e denotes the thickness of the film in the z-direction. The Reynolds number $Re = Lu_L/v$ is based on the length of the film, the take-up velocity and the viscosity of the fluid.

Remark 2.1
Demay and co-workers, see [1, 2], used in their derivation averaged velocities in the xy-plane. This yields a slightly modified momentum equation. Both models clearly predict the edge-bead defect; see Figure 2.

Using the notations of Figure 1, system (1) has to be solved inside the two-dimensional film domain $\Omega = \{(x, y) : 0 < x < L, -W(x) < y < W(x)\}$. Note that the width $W(x)$ of the film is a free boundary and not known *a priori*. The boundary of the domain consists of the extrusion line $\gamma_1 = \{0\} \times (-W(0), W(0))$, the take-up line $\gamma_2 = \{L\} \times (-W(L), W(L))$ and the lateral boundaries $\gamma_3 = (0, L) \times \{-W(x)\}$ and $\gamma_4 = (0, L) \times \{W(x)\}$.

At the inflow boundary, we prescribe a fixed inflow velocity and the initial film thickness

$$(u, v, e) = (u_0, 0, e_0) \quad \text{at } \gamma_1 \tag{2a}$$

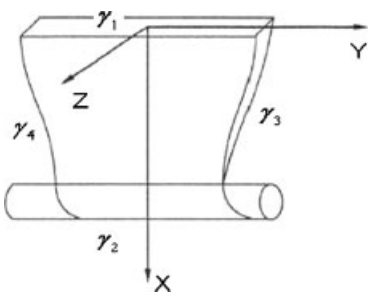

Figure 1. Sketch of the considered geometry for the film casting process.

DOI: 10.1002/fld

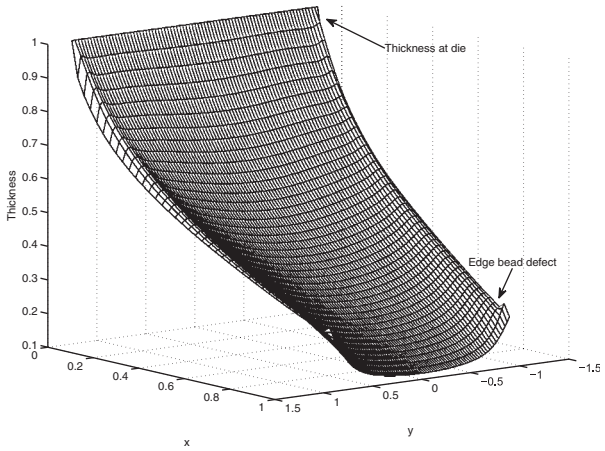

Figure 2. Thickness profile of the film casting process with edge-bead defect.

At the spindle, we also prescribe the winding velocity

$$(u, v) = (u_L, 0) \quad \text{at } \gamma_2 \tag{2b}$$

The ratio $D = u_L/u_0 > 1$ between the winding and the extrusion velocity is also known as the draw ratio. Owing to the hyperbolic nature of Equation (1a), there is no boundary condition for the thickness on γ_2. The treatment of the lateral boundaries γ_3, γ_4 is more sophisticated, since they are free boundaries. Their location is not known in advance and evolves with the width $W = W(x)$ of the film. The dynamic and kinematic conditions along the free boundary read as

$$\sigma \cdot n = 0 \quad \text{at } \gamma_3, \gamma_4 \tag{2c}$$

$$u\partial_x W - v = 0 \quad \text{at } \gamma_3, \gamma_4 \tag{2d}$$

Here n denotes the unit outer normal to γ_i, $i = 3, 4$, and

$$\sigma = (\nabla U) + (\nabla U)^{\mathrm{T}} + 2(\operatorname{div} U)I = \begin{pmatrix} 4\partial_x u + 2\partial_y v & \partial_y u + \partial_x v \\ \partial_y u + \partial_x v & 2\partial_x u + 4\partial_y v \end{pmatrix}$$

is the stress tensor and I is the 2×2 identity matrix.

To simplify notations, we call $z = (u, v, e)$ the state variables of the problem. Typical parameters used throughout this paper are given as follows: stretching distance $L = 0.4\,\mathrm{m}$; film width at the die $W = 1\,\mathrm{m}$; draw ratio $D = 10$; Reynolds number $Re = 3$.

Remark 2.2

Polymeric materials often exhibit a visco-elastic rheological behavior; see, e.g. [5] for a description of the rheology of polymers. However, in this paper we use the simple Newtonian behavior to keep the derivation of the equations short. The proposed optimization method can be applied as well to different constitutive equations; see [6].

DOI: 10.1002/fld

3. OPTIMAL CONTROL

Model (1) is capable of predicting the final thickness $e(L, y)$ of the film. This thickness profile depends on the geometry e_0 of the nozzle as well as the draw ratio D. Using a rectangular nozzle, i.e. a uniform initial thickness e_0, one obtains the well-known effect of edge beads; see Figure 2. In this case the final film is thinner in the middle surface than at the lateral surface, which is an undesired result. In contrast to that, industrial applications aim at producing films with a uniform thickness profile at the take-up roll.

The parameters that can be modified are the initial thickness profile e_0 and the velocity at the die u_0 as well as the velocity of the take-up roll u_L. However, changing the constant velocity at the take-up roll to a non-constant velocity profile is almost impossible under production conditions. Hence, we focus on controlling the initial thickness e_0 and the initial velocity u_0 of the film.

To model the requirement of an even film thickness at the take-up roll, we consider the following tracking-type cost functional:

$$J(z, \varphi) = \|e(L, y) - e_d\|^2 + \alpha \|\varphi\|^2 \tag{3}$$

where e_d is the desired thickness and $\varphi = (e_0, u_0)$ is the control variable of the problem. The term $\|\varphi\|^2$ is necessary in order to prove the existence of optimal control [7] and the parameter $\alpha > 0$ plays the role of a weight. As there is no physical meaning for $\|\varphi\|^2$ in this problem, we consider $\alpha \simeq 0$ so that it will become a negligible quantity in simulation.

The question of minimizing our cost functional $J(z, \varphi)$ belongs to the class of constrained optimization problem, where the cost functional (3) is minimized with respect to the constraint given by the state system (1),

$$\text{minimize } J(z, \varphi) \text{ with respect to } \varphi \text{ subject to (1)} \tag{4}$$

Optimization problems with differential equations constraints have gained a huge interest in the recent years; see [8, 9]. Optimal control problems for the Navier–Stokes equations, or models arising from them, have been investigated in [6, 7, 10]. However, problems with free boundaries are yet a field of research and not much is known about general methods for this situation [11, 12].

In the sequel, we will formally introduce the Lagrangian for problem (4). The first-order optimality system can be derived and leads to the problem of finding the adjoint operator for the state equations (1).

3.1. The first-order optimality system

Let Z denote the space of the state variables $z = (u, v, e)$ and C be the set of admissible controls $\varphi = (e_0, u_0)$, i.e. admissible nozzle shapes e_0 and possible input velocity profiles u_0. Restrictions on the set C of admissible controls might arise from practical considerations, i.e. not all shapes e_0 of the nozzle can be produced. However, to keep the theoretical framework as simple as possible, we do not impose any restrictions on the controls. To shorten the notation, we write the state system (1) together with its boundary conditions (2) shortly as $P(z, \varphi) = 0$, where $P : Z \times C \to W^*$ is called the state operator. Using a set $\xi = (\xi_u, \xi_v, \xi_e) \in W$ of Lagrangian multipliers, we introduce the Lagrangian $L : Z \times C \times W \to \mathbb{R}$ by

$$L(z, \varphi, \xi) = J(z, \varphi) + \langle P(z, \varphi), \xi \rangle_{W^*, W} \tag{5}$$

where $\langle p, \xi \rangle_{W^*, W} \in \mathbb{R}$ denotes the duality pairing between $p \in W^*$ and $\xi \in W$.

DOI: 10.1002/fld

Now, as a standard result from nonlinear optimization, the Karush–Kuhn–Tucker (KKT) system is a necessary first-order optimality condition. Assuming enough regularity, the Lagrangian is Fréchet-differentiable and the first-order optimality condition reads as

$$DL(z, \varphi, \xi) = 0$$

or componentwise

$$P(z, \varphi) = 0 \quad \text{in } W^* \tag{6a}$$

$$\partial_z P^*(\xi)[z, \varphi] + \partial_z J(z, \varphi) = 0 \quad \text{in } Z^* \tag{6b}$$

$$\partial_\varphi P^*(\xi)[z, \varphi] + \partial_\varphi J(z, \varphi) = 0 \quad \text{in } C^* \tag{6c}$$

In system (6), we can easily identify the state (6a), adjoint (6b) and gradient equation (6c) in operator form.

Remark 3.1
To solve the KKT-system (6), we need to derive the adjoint equation (6b) in its strong or at least weak form. Here, the existence of the free boundaries γ_3, γ_4 poses a severe difficulty. Hence, we will derive in the sequel the adjoint equation for our model in the case of fixed boundaries.

This simplification is motivated by the observation that the adjoint variables, as a solution of the adjoint equation, are only needed to compute the direction of the gradient in (6c). When applying a numerical minimization algorithm to (4), we may also work with an inexact, only approximative gradient direction. Hence, we may replace the full adjoint problem, originating for the free boundaries, by a simpler, more tractable one with fixed boundaries. In Section 4, when we present numerical results, we will *a posteriori* justify this approach. We will then see that our algorithm, based only on the inexact gradient information, successfully reduces the cost functional and terminates with a satisfactory solution for the minimization problem.

To derive the adjoint system and gradient equation, we rewrite the state problem (1) in a weak form, multiply by the adjoint variables and integrate over the fixed domain $[0, L] \times [0, W]$. Then we apply the boundary conditions (2a), (2b) and (2c), which read in the case of fixed boundaries γ_3 and γ_4 as

$$\partial_x u + 2\partial_y v = 0, \quad \partial_y u + \partial_x v = 0 \tag{7}$$

Differentiation with respect to the state variables z yields the system of adjoint equations. Assuming enough regularity, we can identify the following strong form:

$$u\partial_x \xi_e + v\partial_y \xi_e = 0 \tag{8a}$$

$$\frac{1}{Re}[4\partial_{xx}\xi_u + \partial_{yy}\xi_u + 3\partial_{xy}\xi_v] + u\partial_x \xi_u + \partial_y(v\xi_u) - \partial_x v\xi_v = e\partial_x \xi_e \tag{8b}$$

$$\frac{1}{Re}[\partial_{xx}\xi_v + 4\partial_{yy}\xi_v + 3\partial_{xy}\xi_u] + \partial_x(u\xi_v) + v\partial_y \xi_v - \partial_y u\xi_u = e\partial_y \xi_e \tag{8c}$$

DOI: 10.1002/fld

together with the boundary conditions

$$\xi_e(L, y) = \frac{2(e(L, y) - e_d)}{u_L} \tag{8d}$$

$$\xi_u(0, y) = \xi_v(0, y) = 0, \quad \xi_u(L, y) = \xi_v(L, y) = 0 \tag{8e}$$

$$\frac{1}{Re}\left[\partial_y \xi_u - \frac{7}{2}\partial_x \xi_v\right] + v\xi_u = 0, \quad \frac{4}{Re}[\partial_x \xi_u - \partial_y \xi_v] - v\xi_v = e\xi_e \quad \text{on } \gamma_3 \text{ and } \gamma_4 \tag{8f}$$

Taking the derivative of the Lagrangian L with respect to the control variable e_0 and u_0 yields the gradient equations (9a) and (9b), respectively,

$$\int_{-W}^{W} \xi_e(0, y) u_0 \, dy = 0 \tag{9a}$$

$$\int_{-W}^{W} \xi_e e_0 - \frac{4}{Re}\frac{\partial \xi_u}{\partial x}(0, y) = 0 \tag{9b}$$

4. NUMERICAL SIMULATIONS

The KKT-system (6) corresponding to the first-order optimality conditions for the minimization problem (4) is a system of coupled, nonlinear PDEs. Hence, we will apply an iterative algorithm to solve them.

4.1. Solution algorithm

Starting from an initial guess for e_0 and u_0 we compute the state variables z from the nonlinear state equations. With this new state one can continue to solve the adjoint system for ξ. Using the state and adjoint variables we are able to update the control variables e_0 and u_0. The detailed algorithm reads as

1. Given initial controls e_0^0 and u_0^0, set $k = 0$.
2. Solve the state equations (6a), i.e. (1) with the boundary conditions (2) as a free boundary value problem to obtain the new state variables z^{k+1}.
3. Given the state z^{k+1} corresponding to the controls e_0^k and u_0^k, solve the adjoint problem (6b), i.e. (8) as a fixed boundary value problem to obtain ξ^{k+1}.
4. Given ξ^{k+1}, update the control by

$$e_0^{k+1}(y) = e_0^k(y) - \xi_e^{k+1}(0, y) u_0^k(y) \tag{10a}$$

$$u_0^{k+1}(y) = u_0^k(y) - \xi_e^{k+1}(0, y) e_0^k(y) + \frac{4}{Re}\frac{\partial \xi_u^{k+1}}{\partial x}(0, y) \tag{10b}$$

5. Calculate the cost functional $J^{k+1} = J(z^{k+1}, \phi^{k+1})$
6. If $J^{k+1} < \varepsilon$
   then *Stop*
   else set $k = k + 1$ and go to step 2.

DOI: 10.1002/fld

Remark 4.1
In Equations (10a) and (10b) one might add a suitable step size for the updated controls to improve the convergence behavior of the algorithm. Possible choices are an Armijo-type update or an approximate line-search algorithm. For details refer to [13]. The numerical results given in Section 4.4 were obtained using the above algorithm.

4.2. Solving the state equation

As the boundaries γ_3 and γ_4 are free surfaces, it is difficult to implement the boundary condition $\sigma \cdot n = 0$. To overcome the free surface, we transform the domain into a square domain by mapping the coordinates (x, y) to $(x, \tilde{y})$ where $\tilde{y}(x) = y/W(x)$. Then, the new coordinates belong to a square domain $(x, \tilde{y}) \in [0, L] \times [-1, 1]$. Applying this coordinate transformation to the state system (1) yields

$$\partial_x(eu) - \tilde{y}\frac{W'}{W}\partial_y(eu) + \frac{1}{W}\partial_y(ev) = 0 \tag{11a}$$

$$\begin{aligned} &u\partial_x u + \frac{v}{W}\partial_{\tilde{y}} u - u\tilde{y}\frac{W'}{W}\partial_{\tilde{y}} u \\ &\quad = \frac{1}{Re}\left[4\partial_{xx} u + \frac{1}{W^2}\partial_{\tilde{y}\tilde{y}} u + \frac{3}{W}\partial_{x\tilde{y}} v - 8\tilde{y}\frac{W'}{W}\partial_{x\tilde{y}} u - 4\tilde{y}\frac{W''}{W}\partial_{\tilde{y}} u\right. \\ &\qquad \left. + 4\tilde{y}\frac{(W')^2}{W^2}\partial_{\tilde{y}} u + 4\tilde{y}^2\frac{(W')^2}{W^2}\partial_{\tilde{y}\tilde{y}} u - 3\tilde{y}\frac{W'}{W^2}\partial_{\tilde{y}\tilde{y}} v - 3\frac{W'}{W^2}\partial_{\tilde{y}} v\right] \end{aligned} \tag{11b}$$

$$\begin{aligned} &u\partial_x v + \frac{v}{W}\partial_{\tilde{y}} v - u\tilde{y}\frac{W'}{W}\partial_{\tilde{y}} v \\ &\quad = \frac{1}{Re}\left[4\partial_{xx} v + \frac{4}{W^2}\partial_{\tilde{y}\tilde{y}} v + \frac{3}{W}\partial_{x\tilde{y}} u - 2\tilde{y}\frac{W'}{W}\partial_{x\tilde{y}} v - \tilde{y}\frac{W''}{W}\partial_{\tilde{y}} v\right. \\ &\qquad \left. + \tilde{y}\frac{(W')^2}{W^2}\partial_{\tilde{y}} v + \tilde{y}^2\frac{(W')^2}{W^2}\partial_{\tilde{y}\tilde{y}} v - 3\tilde{y}\frac{W'}{W^2}\partial_{\tilde{y}\tilde{y}} u - 3\frac{W'}{W^2}\partial_{\tilde{y}} u\right] \end{aligned} \tag{11c}$$

As the flow is symmetric about the centerline $y = 0$, it is sufficient to solve the problem in the half domain $[0, L] \times [0, 1]$. The boundaries of the computational domain are the extrusion line $\gamma_1 = \{0\} \times [0, 1]$, the take-up line $\gamma_2 = \{L\} \times [0, 1]$ and the former free surface $\gamma_3 = [0, L] \times \{1\}$. The fourth boundary $\gamma_4 = [0, L] \times \{0\}$ is the symmetry line. The conditions at the boundaries read as

$$u = u_0, \quad v = 0, \quad e = e_0 \text{ at } \gamma_1 \tag{12a}$$

$$u = u_L, \quad v = 0 \text{ at } \gamma_2 \tag{12b}$$

$$u(x, y) = u(x, -y), \quad v(x, y) = -v(x, -y), \quad e(x, y) = e(x, -y) \text{ at } \gamma_4 \tag{12c}$$

$$\frac{1}{W}\partial_{\tilde{y}} u + \partial_x v - \tilde{y}\frac{W'}{W}\partial_{\tilde{y}} v = 0, \quad \frac{2}{W}\partial_{\tilde{y}} v + \partial_x u - \tilde{y}\frac{W'}{W}\partial_{\tilde{y}} u = 0 \text{ at } \gamma_3 \tag{12d}$$

The film width $W(x)$ is computed using the kinematic condition (2d), i.e. $W' = v/u$ and $W(0) = W_0$.

DOI: 10.1002/fld

In the numerical algorithm, we solve system (11b) and (11c) for the velocities u and v. Later, we update the film width W. These steps are iterated until convergence is reached. Then, we compute the film thickness using (11a).

Remark 4.2
If we use system (11) and (12) to derive the adjoint and gradient equation, we get the exact adjoint gradient equation. However, the adjoint system will have a rather complicated structure and hence it will be difficult and expensive to solve. Therefore, we prefer to work with the inexact adjoint system (8), which is cheaper to solve. The price for the reduced complexity of the adjoint system is an increase in the number of iterations needed to solve the full KKT-system (6).

4.3. Discretization

For the numerical simulations we use standard finite differences on a uniform grid with mesh widths $h, k>0$ in the x- and $\tilde{y}$-directions, respectively. The same grid is used for the state as well as for the adjoint equations. We use the standard notation u_{ij} to denote the value of the function u at the grid point $(x_i, \tilde{y}_j)=(ih, jk)$. For the hyperbolic equations (11a) and (8a) we apply upwind methods. In Equation (11a) governing the film thickness, the flow is oriented in the positive x-direction (Figure 3); hence the upwind scheme reads as

$$\frac{(eu)_{ij}-(eu)_{i-1j}}{h}-y\frac{W'}{W}\frac{(eu)_{ij+1}-(eu)_{ij-1}}{2k}+\frac{1}{W}\frac{(ev)_{ij+1}-(ev)_{ij}}{k}=0$$

In the case of the adjoint thickness equation (8a) the information is travelling in the reverse direction (Figure 4) and hence the upwind discretization reads as

$$u_{ij}\frac{(\xi_e)_{i+1j}-(\xi_e)_{ij}}{h}+v_{ij}\frac{(\xi_e)_{ij}-(\xi_e)_{ij-1}}{k}=0$$

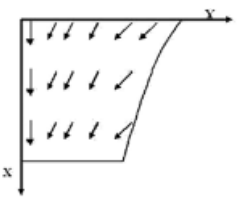

Figure 3. Flow direction in the state system.

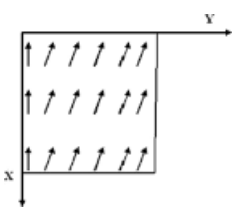

Figure 4. Flow direction in the adjoint system.

DOI: 10.1002/fld

In the velocity equations (11b) and (11c) the nonlinear terms are handled by iteration. Central differences are used to discretize the derivatives. The adjoint equations (8b) and (8c) are discretized analogously.

4.4. Simulation results

In a first step, we solved the state system (1) or respectively (11) for a given constant initial thickness e_0. Figure 2 shows the thickness of the film. The transversal velocity component v is shown in Figure 5. Figure 5 plots the transversal velocity $v(x,\cdot)$ at different lateral cuts $y=y_i$.

In Figure 5 the velocities are negative, implying that the fluid moves towards the centerline $y=0$; this yields the neck-in of the film. This neck-in is also clearly visible in Figure 6 showing the evolution of the width of the film. The centerline of the film, i.e. $y=0$, corresponds to the velocity $v=0$ and the edge or boundary of the film corresponds to the curve with maximum velocity. Along the central part of the film, i.e. close to the centerline, the transversal velocity component

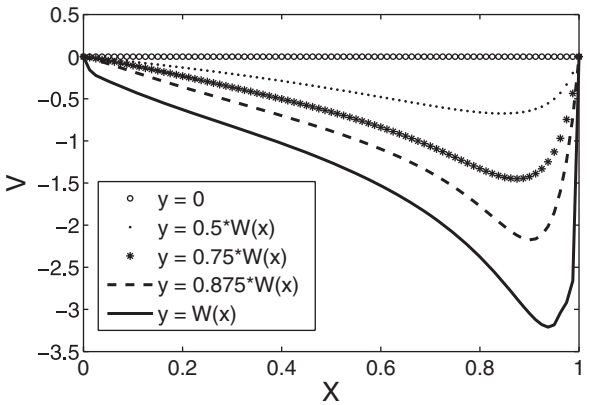

Figure 5. Transversal velocity v.

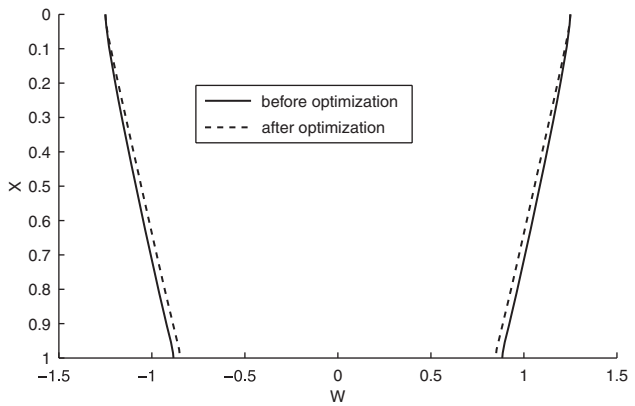

Figure 6. Film width w.

DOI: 10.1002/fld

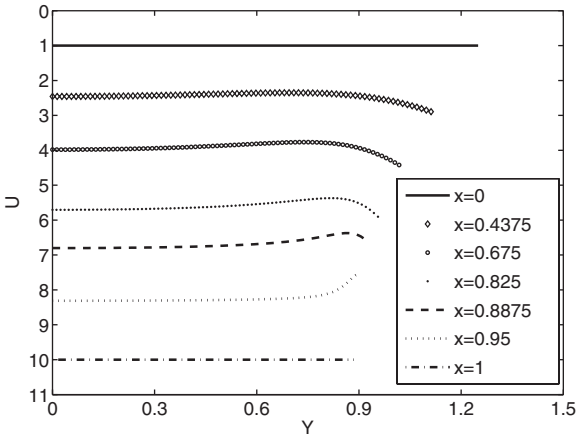

Figure 7. Longitudinal velocity u.

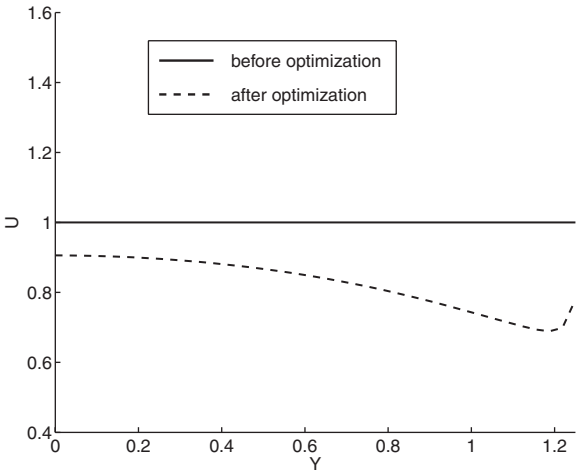

Figure 8. Initial velocity profile u_0 before and after optimization.

v is rather small. Hence, we may conclude that in the central part of the film mainly uniaxial extension occurs, i.e. just a stretching in the longitudinal direction. Along the edges of the film, biaxial extension is predominant leading to a stretching and necking-in of the film. Figure 7 shows the longitudinal velocity component $u(\cdot, y)$ at different lateral cuts. The increase in the longitudinal velocity due to the draw ratio $D>1$ is clearly visible.

Finally, we investigated the result of the optimization problem (4). The aim was to find an initial velocity profile u_0 and the shape of the nozzle (i.e. an initial thickness e_0 of the film), so that we obtain a uniform thickness e_d at the position of the spindle. Figure 8 shows the initial velocity profile u_0 before and after optimization. From Figure 8 it is clear that the velocity at the edge of the film should be less compared with the center part of the film, so that the flux in the edge

DOI: 10.1002/fld

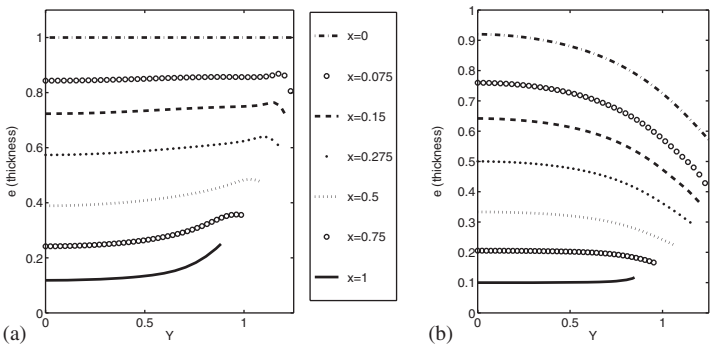

Figure 9. Film thickness e before optimization (a) and after optimization (b).

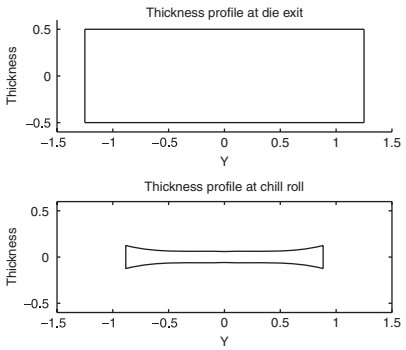

Figure 10. Nozzle shape (top) and film thickness at take-up (bottom) before optimization.

part will be less and it results in stopping the accumulation of fluid in the edge and removes the edge bead. Figure 9(a) shows the thickness profile for un-optimized situation. Lateral cuts of the film thickness $e(\cdot, y)$ are plotted for different x-coordinates along the film. Two effects are clearly visible from this figure: on the one hand, the decrease in the film thickness along the centerline $y=0$, and on the other hand, the development of the edge-bead effect as the longitudinal coordinate x grows. In contrast to that, Figure 9(b) shows the situation with the optimized initial thickness e_0. The uppermost line corresponds to the initial thickness e_0 and the graph at the bottom shows the film thickness at the take-up point $x=L$. At the take-up point we obtain a constant film thickness of $e_d=0.1$ corresponding to the draw ratio $D=10$. Figures 10 and 11 show a comparison of the un-optimized (left) and optimized situation (right). The initial thickness corresponding to the shape of the nozzle is shown in the upper part and the final film thickness is given below. In the optimized situation the close-to ellipsoidal shape of the nozzle with the modified initial velocity u_0 given in the Figure 8 counterbalances the edge-bead effect resulting in a uniform film thickness.

Remark 4.3

The results shown in Figures 10 and 11 may serve as an *a posteriori* justification of our inexact adjoint system (8). Recall that we solve the state equation (1) as a free boundary value problem,

DOI: 10.1002/fld

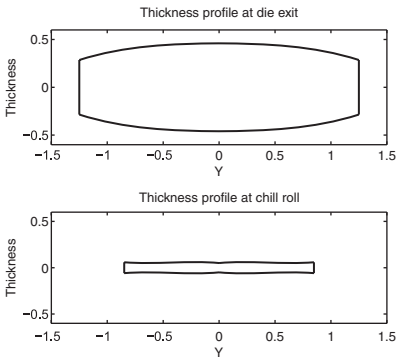

Figure 11. Nozzle shape (top) and film thickness at take-up (bottom) after optimization.

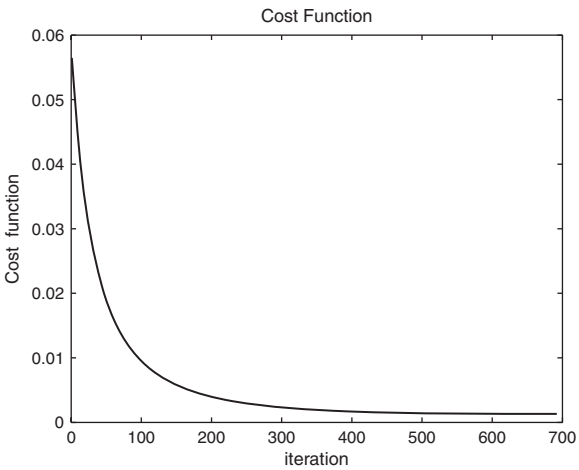

Figure 12. Decrease of the cost functional (3) versus iteration number.

but the adjoint system on a fixed domain with a uniform film width. This leads to an inexact computation of the gradient and hence an inexact update of the control variable in Equation (10a). However, this inexact update still leads to a decrease in the cost functional and our optimization algorithm terminates with an acceptable solution solving problem (4). The optimized final thickness of the film is constant at the take-up point. Hence, the optimization algorithm—with the inexact gradient information—has terminated at the minimum of our cost functional (3). Figure 12 shows the decrease in the cost functional versus the iteration number. A rigorous justification of the observed convergence to the minimum based on space-mapping techniques is left open for future research.

To end our investigations of the optimization problem, the following table shows the computational time and the number of iterations required for different tolerance levels ε.

DOI: 10.1002/fld

ε	Number of iterations	Time (min)
0.05	6	2
0.01	96	18
0.005	169	27
0.001	692	52

5. CONCLUSION

We studied the isothermal film casting process. Based on the averaged Navier–Stokes equations, the evolution of the film thickness and width is governed by a free boundary value problem. In an industrial application of the film casting process, one is typically interested in obtaining an even thickness distribution at the take-up point of the film. However, a uniform thickness profile at the nozzle always leads to the so-called edge-bead effect; the final film gets thinner in the middle than at the edges. Hence, we formulated an optimization problem to determine the optimal velocity profile at the nozzle and shape of the nozzle, which will lead to an even thickness distribution at the take-up point. Applying the Lagrangian formalism to a modified problem with fixed film width, we were able to derive an approximate adjoint equation. This approximate adjoint was used to set up an minimization algorithm for our problem. Numerical simulations show that, even with this approximate version of the adjoint equations, the minimization algorithm converges. Therefore, we were able to compute the optimal shape of the nozzle that produces a uniform film thickness.

A mathematical analysis of the proposed approximative adjoint equations and their relation to the full adjoint equations for the free boundary value problem is left as an open question subject to future research.

ACKNOWLEDGEMENTS

The authors thank the anonymous referees for their valuable comments.

REFERENCES

1. d'Halewyu S, Agassant JF, Demay Y. Numerical simulation of the cast film process. *Polymer Engineering and Science* 1990; **30**:335–340.
2. Silagy D, Demay Y, Agassant JF. Numerical simulation of the film casting process. *International Journal for Numerical Methods in Fluids* 1999; **30**:1–18.
3. Fortin A, Carrier P, Demay Y. Numerical simulation of coextrusion and film casting. *International Journal for Numerical Methods in Fluids* 1995; **20**:31–57.
4. Barq P, Haudin JM, Agassant JF. Isothermal and anisothermal models for cast film extrusion. *International Polymer Processing* 1992; **VII**(4):334–349.
5. Bird RB, Armstrong RC, Hassager O. *Dynamics of Polymeric Liquids*, vol. 1. Wiley: New York, 1977.
6. Kunisch K, Marduel X. Optimal control of non-isothermal viscoelastic fluid flow. *Journal of Non-Newtonian Fluid Mechanics* 2000; **88**(3):261–301.
7. Abergel F, Temam R. On some control problems in fluid mechanics. *Theoretical and Computational Fluid Dynamics* 1990; **1**:303–325.
8. Hinze M, Volkwein S. Instantaneous control for the instationary Burgers equation—convergence analysis and numerical implementation. *Nonlinear Analysis—Theory Methods and Applications* 2002; **50**:1–26.

DOI: 10.1002/fld

9. Goldberg H, Troeltzsch F. On a Lagrange–Newton method for a nonlinear parabolic boundary control problem. *Optimization Methods and Software* 1998; **8**:225–247.
10. Gunzburger MD, Hou LS, Manservisi S, Yan Y. Computations of optimal controls for incompressible flows. *International Journal of Computational Fluid Dynamics* 1998; **11**:181–191.
11. Hinze M, Ziegenbalg S. Optimal control of the free boundary in a two-phase Stefan problem with flow driven by convection. *Zeitschrift fur Angewandte Mathematik und Mechanik* 2007; **87**(6):430–448.
12. Hinze M, Ziegenbalg S. Optimal control of the free boundary in a two-phase Stefan problem. *Journal of Computational Physics* 2007; **223**(2):657–684.
13. Kelley CT. *Iterative Methods for Optimization*. SIAM: Philadelphia, PA, 1999.

DOI: 10.1002/fld